ACS Medicinal Chemistry Letters

pubs.acs.org/acsmedchemlett Letter

# Discovery of CVN293, a Brain Permeable KCNK13 (THIK-1) Inhibitor Suitable for Clinical Assessment

Roland W. Bürli,[‖] Kevin J. Doyle,[‖] Louise Dickson, Anna Rowland, Kim Matthews, Andrew J. Stott, Martin Teall, Bernardino Ossola, Samuel G. Russell, Jenna R. M. Harvey, Yiming Wu, Lakshminarayana Narayana, Nicola L. Brice, Mark Carlton, and Lee A. Dawson*

Cite This: https://doi.org/10.1021/acsmedchemlett.4c00035 Read Online

ACCESS | Metrics & More | Article Recommendations | Supporting Information

**ABSTRACT:** The potassium ($K^+$) ion channel KCNK13 is specifically expressed in human microglia with elevated expression observed in post-mortem human brain tissue from patients with Alzheimer's disease. Modulation of KCNK13 activity by a small-molecule inhibitor is proposed as a potential treatment for neurodegenerative diseases. Herein, we describe the evolution of a series of KCNK13 inhibitors derived from a high-throughput screening campaign, resulting in **CVN293**, a potent, selective, and brain permeable clinical candidate molecule. **CVN293** demonstrated a concentration-dependent inhibition of the NLRP3-inflammasome mediated production of IL-1$\beta$ from LPS-primed murine microglia. Cross-species pharmacokinetic data of **CVN293** are also disclosed. These findings support the advancement of **CVN293** in clinical trials.

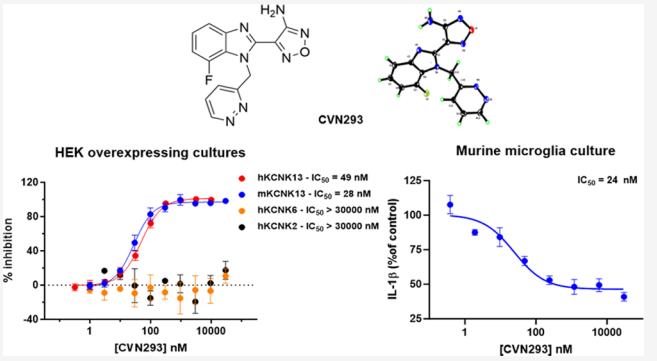


**KEYWORDS:** *Neuroinflammation, KCNK13 (THIK-1) inhibitor, microglia, neurodegeneration, NLRP3, IL-1β*



Genetic ablation of NLRP3 or pharmacological blockade of the NLRP3-inflammasome has produced significant improvements in ongoing disease pathology in numerous preclinical models of neurodegenerative diseases such as Alzheimer's disease, Parkinson's disease, and ALS.[1,2] This finding suggests that modulating NLRP3 inflammasome-induced neuroinflammation may provide a biochemical intervention point of potential therapeutic benefit. Indeed, several NLRP3-inflammasome inhibitors have been developed and are currently being investigated in clinical trials for peripheral as well as central disorders.[3] While NLRP3 is expressed in microglia and macrophages, KCNK13 expression appears to be largely restricted to microglia in humans with little peripheral occurrence (www.proteinatlas.org).

The role of $K^+$ efflux in canonical NLRP3 activation, in response to many stimuli, is well documented, and several ion channels have been suggested to mediate this $K^+$ current in microglia. One such channel is encoded by the KCNK13 ($K_{2P}13.1$) gene, which translates to a two-pore forming domain $K^+$ channel, also known as THIK-1.[4,5] We previously showed that, when **N**uclear **E**nriched **T**ranscript **S**ort **SEQ**uencing (NETSseq) is used,[6] KCNK13 is specifically expressed in human microglia and transcript levels increase in microglial nuclei isolated from post-mortem brain tissue from patients with Alzheimer's disease compared to nonaffected control donors.[7] This observation has been confirmed by a recent study demonstrating a significant increase in RNA and reduction in DNA methylation of KCNK13 in brain tissue from patients with Alzheimer's and Parkinson's disease.[8] Taken together, these findings suggest that specific pharmacological targeting of KCNK13 may provide a therapeutic strategy for attenuating microglial NLRP3-mediated proinflammatory processes that underlie the ongoing progression of multiple neurodegenerative diseases.

We previously reported the identification and characterization of the KCNK13 inhibitors **1** and **2** (Figure 1), which were discovered in a high-throughput screening campaign.[7] The benzimidazolyl-oxadiazole **1** was characterized as a potent inhibitor of human and mouse KCNK13 ($IC_{50}$ values 46 and 49 nM, respectively).[7] Further, in primary mouse microglia, compound **1** evoked a concentration-dependent inhibition of IL-1$\beta$ release ($IC_{50}$ 106 nM).[7]

Herein, we describe the evolution of these early molecules to the identification of our clinical candidate **CVN293**, a potent,

Received: January 22, 2024
Revised: March 23, 2024
Accepted: March 26, 2024




https://doi.org/10.1021/acsmedchemlett.4c00035
ACS Med. Chem. Lett. XXXX, XXX, XXX−XXX

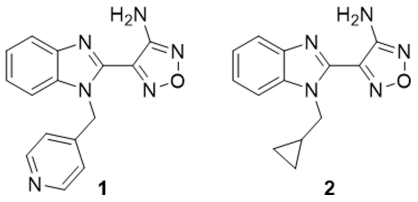

**Figure 1.** Previously reported KCNK13 inhibitors.

selective, and brain permeable KCNK13 inhibitor. To the best of our knowledge, these benzimidazoles represent the only known small molecule inhibitors of KCNK13, underpinning how underexplored this ion channel is.

We aimed to develop a potent, selective, and brain permeable KCNK13 inhibitor to combat neuroinflammation in patients suffering from neurodegenerative diseases. In addition, a molecule intended for these patient populations should be orally bioavailable and exhibit an appropriate safety profile.

The cyclopropyl compound **2** (Figure 1) is a known kinase inhibitor, and a crystal structure determining its binding mode to the p70-S6K1 chimera has been reported.[9] In contrast, the pyridyl analog **1** was devoid of any measurable kinase activity, presumably due to the larger steric influence of the heteroaromatic substitution, and therefore served as a promising starting point for further optimization. As previously discussed, this pyridine **1** demonstrated good distribution to the CNS compartment, which is commensurate with its physicochemical properties, resulting in an excellent CNS MPO[7] score of 5.64. However, it exhibited high clearance in the presence of liver microsomes, which correlated well with its high in vivo clearance in rodents. Thus, our objective was to improve the metabolic stability and PK profile of analogs of **1**, while retaining the encouraging KCNK13 potency. We started by investigating the role of the amino-oxadiazole unit in **1**; the in vitro biological activity of selected analogs is summarized in Table 1. Acylation of the exocyclic amino group in **1** led to the complete loss of KCNK13 inhibition of the acetamide **3**, whereas replacement of the $NH_2$ group by a methyl substituent surprisingly retained good activity ($IC_{50}$ 89 nM for the methyl analog **4**). Introduction of other five-membered heterocycles to replace the oxadiazole ring generally led to a loss of desired KCNK13 inhibition as exemplified by the imidazole **5**, the less basic pyrazole **6**, and oxazole **7**. Several six-membered rings were tested, which were all significantly less potent KCNK13 inhibitors than the oxadiazoles **1** and **4** (data not shown); the amino-pyridine **8**, which is structurally the closest derivative of **1**, showed no activity up to 22 $\mu$M and is shown as a representative example.

Various substituents at the benzimidazole core were explored with the aim of improving the metabolic stability of these molecules; unfortunately, these modifications generally led to a significant reduction in potency (data not shown), and the only substituent tolerated without a loss of KCNK13 inhibitory activity was a fluoride. As shown in Table 2, the regioisomers **9**–**12** bearing a fluoride substituent in positions 4–7 of the benzimidazole scaffold were all potent KCNK13 inhibitors. Compounds **9**–**11** displayed moderate intrinsic clearance ($Cl_{int}$) in human, rat, and mouse liver microsomes, whereas compound **12** was the only regioisomer to display low microsomal turnover in the mouse ($Cl_{int}$ = 14 $\mu$L/min/mg). The benzimidazole analogs **9**–**11** displayed low aqueous solubility below micromolar concentrations at neutral pH, with compound **12** as the only analog with measurable aqueous solubility (3.7 $\mu$M).

**Table 1. Investigation of Amino-Oxadiazole Replacements**

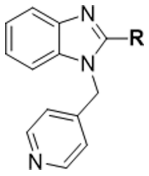

| Cpd | R | hKCNK13 $IC_{50}$ ($\mu$M) | HLM RLM[a] |
|---|---|---|---|
| **1** |  | 0.046 | 24<br>56 |
| **3** |  | >22 | 34<br>45 |
| **4** |  | 0.089 | 45<br>47 |
| **5** |  | 3.43 | n.d. |
| **6** |  | 9.20 | n.d. |
| **7** |  | 2.94 | n.d. |
| **8** |  | >22 | n.d. |

[a]HLM (human liver microsomes) and RLM (rat liver microsomes), $Cl_{int}$ in $\mu$L/min/mg. n.d. not determined.

**Table 2. Effect of Substituents at the Benzimidazole Core**

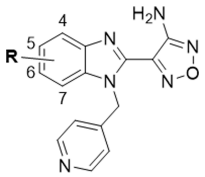

| Cpd | position of F | hKCNK13 $IC_{50}$ ($\mu$M) | RLM MLM[a] HLM | solubility ($\mu$M)[b] |
|---|---|---|---|---|
| **9** | 4 | 0.055 | 27<br>74<br>25 | <0.3 |
| **10** | 5 | 0.042 | 14<br>28<br>19 | <0.3 |
| **11** | 6 | 0.034 | 10<br>58<br>37 | <0.3 |
| **12** | 7 | 0.046 | 22<br>66<br>14 | 3.7 |

[a]HLM, RLM, MLM: human, rat, and mouse liver microsomes, $Cl_{int}$ in $\mu$L/min/mg. [b]Kinetic aqueous solubility (pH = 7.4).

As compound **12** showed the lowest intrinsic clearance in the presence of mouse liver microsomes and was the most soluble



https://doi.org/10.1021/acsmedchemlett.4c00035
ACS Med. Chem. Lett. XXXX, XXX, XXX−XXX

**Table 3. Effect of Substituents at the Benzimidazole Core on the Potency and DMPK Properties**

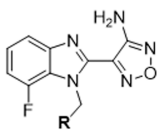


generic structure for **13**-**18**

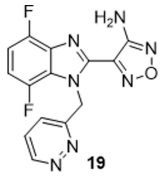


**19**

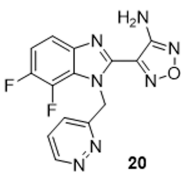


**20**

| Cpd | R | KCNK13 $IC_{50}$ (μM) human | KCNK13 $IC_{50}$ (μM) mouse | HLM RLM MLM[a] | mPPB ($f_u$, %)[b] | mBTB ($f_u$, %)[c] | sol. (μM)[d] | unbound conc. (μM; mouse)[e] plasma | unbound conc. (μM; mouse)[e] brain | Kp $Kp_{u,u}$ (4 h) |
|---|---|---|---|---|---|---|---|---|---|---|
| **13** |  | 0.047 | 0.062 | 21<br>68<br>50 | 13.8 | 7.7 | 10 | 0.009 | 0.018 | 0.56<br>2.2 |
| **14** |  | 0.049 | 0.026 | 10<br>24<br>18 | 12.9 | 5.7 | 6.5 | n.d. | n.d. | n.d. |
| **15** | 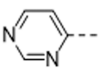 | 0.046 | n.d. | 10<br>77<br>30 | 11.1 | 9.1 | 9.9 | n.d. | n.d. | n.d. |
| **16** | 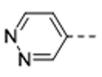 | 0.050 | n.d. | 9.6<br>31.6<br>13.9 | 18.8 | 12.8 | 10.4 | 0.009 | 0.018 | 0.68<br>1.9 |
| **CVN293** | 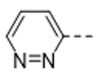 | 0.041 | 0.028 | <9.6<br>9.9<br><9.6 | 17.3 | 13.6 | 94 | 0.372 | 0.248 | 0.84<br>0.66 |
| **17** | 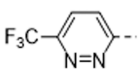 | 0.084 | 0.074 | 18.3<br>n.d.<br>245 | 3.5 | 2.4 | 1.6 | n.d. | n.d. | n.d. |
| **18** | 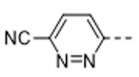 | 0.050 | 0.035 | 9.6<br>40<br>37 | 7.1 | 6.4 | 8.4 | n.d. | n.d. | n.d. |
| **19** | see Fig | 0.037 | 0.042 | 9.6<br>12.6<br>10.1 | 15.9 | 13.0 | 12.9 | 0.793 | 0.630 | 0.96<br>0.80 |
| **20** | | 0.050 | n.d. | <9.6<br>15.4<br><9.6 | 16.1 | 9.7 | 3.9 | 0.080 | 0.056 | 1.17<br>0.7 |

[a]HLM, RLM, MLM: human, rat, or mouse liver microsomes, $Cl_{int}$ in μL/min/mg. [b]Mouse plasma protein binding (mPPB). [c]Mouse brain tissue binding (mBTB) assessed by equilibrium dialysis. [d]Kinetic aqueous solubility (pH = 7.4). [e]Calculated from brain and plasma levels at 4 h following a 10 mg/kg p.o. dose.

analog, we chose to keep the 7-fluoro substituent intact and investigate a series of methylene linked six-membered heterocyclic derivatives. To improve the solubility and metabolic stability of these compounds, we focused on heterocyclic groups containing a second ring nitrogen. As shown in Table 3, the potency of most analogs was well below 100 nM and, in line with the relatively high homology between human and mouse KCNK13 (85% amino acid identity), an excellent correlation of on-target activity across species was observed. Notably, the binding site of these compounds within the ion channel is not known at this stage. All tested compounds demonstrated high unbound fractions in mouse and human plasma, ranging from 3.5 to 18.8%, and relatively low nonspecific brain tissue binding with unbound fractions in brain tissue between 2.4 and 13.6%. Selected compounds were advanced into a brain distribution study whereby test articles were orally administered to mice at a 10 mg/kg dose and brain and plasma concentrations were measured 4 h post dosing. Unbound plasma and brain concentrations were calculated using the respective unbound fractions, as measured in a separate in vitro equilibrium dialysis study. The objective of this study was to determine the ratios of brain to plasma concentrations of the different compounds as well as the unbound brain concentration 4 h post dosing. The pyrazine **13** and the pyrimidine **14** both retained human KCNK13 potency but with no general improvement in kinetic solubility at pH 7.4 or liver microsomal stability. In an exploratory tissue distribution study in mice, compound **13** showed very little unbound brain or plasma concentration at 4 h post dosing, in line with its relatively high metabolic turnover in the presence of mouse liver microsomes. The regioisomeric pyrimidine **15** showed characteristics very similar to those of **14** and was not profiled further. Pyridazine **16** displayed somewhat improved mouse liver microsomal stability; however, exposure levels were low in mice 4 h after oral gavage.



https://doi.org/10.1021/acsmedchemlett.4c00035
ACS Med. Chem. Lett. XXXX, XXX, XXX−XXX

In contrast, the isomeric **CVN293** demonstrated markedly improved metabolic stability across human, rat, and mouse liver microsomes, resulting in unbound brain concentrations at the 4 h time point, ~10-fold over its in vitro $IC_{50}$ value. The $Kp_{u,u}$ value of 0.66 that was obtained from this experiment confirmed the good brain permeability of this compound in mice, and pleasingly, this molecule also showed the highest kinetic solubility (94 $\mu$M) observed in this chemical series. Unfortunately, substitution of the pyridazine moiety to block a potential metabolic soft spot next to the ring nitrogen by either a $CF_3$ group (**17**) or a nitrile function (**18**) reduced the metabolic stability and aqueous solubility. Given the tolerance of fluorine atoms at the benzimidazole core, we tested several disubstituted analogs; both difluoro benzimidazoles **19** and **20** were characterized with good in vitro potency, high in vitro metabolic stability, and low nonspecific binding to brain and plasma protein. In the tissue distribution study, compound **19** exhibited a slightly higher unbound brain concentration than **CVN293**. Therefore, we decided to advance both **19** and **CVN293** in a full pharmacokinetic study. However, the oral bioavailability of compound **19** was only 8% compared to 87% for **CVN293**, which may in part be a consequence of the low aqueous solubility of **19**. Based on this observation, **CVN293** was selected for further profiling.

In line with its good brain permeability, **CVN293** has high in vitro permeability ($P_{app}$ A to B: 41 × $10^{-6}$ cm/s) and is not subject to active efflux by transport systems such as P-gp or BCRP. Hepatic metabolism is likely to be the major route of clearance for **CVN293** characterized in vitro by low metabolism in liver microsomes, moderate to high metabolism in hepatocytes, and no evidence of metabolism by aldehyde oxidase in liver cytosol. While some reversible CYP450 inhibition was observed for CYP1A2, there was no TDI observed across the panel of CYP450 isoforms tested.

Compound **CVN293** exhibits a calculated polar surface area of 108.8 $Å^2$, which is considered to be high for a brain permeable molecule. We rationalized the high CNS distribution of this molecule by an intramolecular hydrogen bond between the exocyclic amino group and a ring nitrogen of the benzimidazole unit, leading to an overprediction of the polar surface area. This H-bond has been confirmed by a single crystal structure, as shown in Figure 2. As a result, the biaryl system adopts a planar conformation while the pyridazine unit is rotated out of the biaryl plane.

The PK parameters following a single oral or i.v. administration to rats, dogs, or non-human primates (cynomolgus monkeys) are summarized in Table 4.

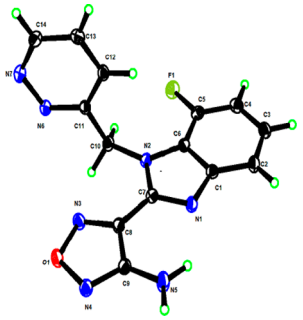

**Figure 2.** Single crystal X-ray structure confirming the intramolecular hydrogen bond in **CVN293**.

**Table 4. Pharmacokinetic Data of CVN293 Across Species**

| | rat | | dog | | cynomolgus monkey | |
|---|---|---|---|---|---|---|
| | i.v. | p.o. | i.v. | p.o. | i.v. | p.o. |
| dose (mg/kg) | 0.5[a] | 3 | 1[b] | 10 | 1[b] | 3 |
| $Cl_p$ (mL/min/kg) | 35 | | 38 | | 22 | |
| $Vd_{ss}$ (L/kg) | 1.85 | | 1.42 | | 1.45 | |
| $C_o$ (ng/mL) | 304 | | 626 | | 896 | |
| $C_{max}$ (ng/mL) | | 468 | | 241 | | 165 |
| $T_{max}$ (h) | | 1.0 | | 1.25 | | 1.0 |
| $AUC_{0\rightarrow\infty}$(ng·h/mL) | 222 | 1,236 | 438 | 630 | 782 | 546 |
| $t_{1/2}$ (h) | 1.0 | 2.0 | 0.5 | 2.6 | 1.1 | 1.9 |
| $F$ (%) | | 87 | | 41 | | 24 |

[a]Formulation: 5% DMSO, 5% solutol, 90% $H_2O$. [b]Formulation: 5% DMSO, 10% solutol, 85% $H_2O$.

Plasma clearance was moderate in Sprague−Dawley rats and cynomolgus monkeys (35 and 22 mL/min/kg, respectively), translating to ~50% of each species' respective hepatic blood flow values, while clearance was greater than hepatic blood flow in beagle dogs at 38 mL/min/kg. The volume of distribution ($Vd_{ss}$) was similar across species and greater than body water volume, thereby demonstrating good distribution of **CVN293** in the body. Following a single i.v. dose, the half-life ($t_{1/2}$) in beagle dogs, Sprague−Dawley rats, and cynomolgus monkeys varied (0.5, 1.0, and 1.1 h, respectively), likely due to the differential clearance across these species. After a single oral dose, absorption of the test article was rapid, with $T_{max}$ranging from 1 to 1.25 h in all species. The extent of absorption and bioavailability was characterized as moderate to high with bioavailability values ranging from 24% (cynomolgus monkey) to 41% (dog) and 87% (rat) across species. We found that bioavailability was dependent on particle size in rats and dogs, and lower oral bioavailability values were observed when using nonmicronized material. Notably, the monkey study was only performed with nonmicronized material, and the oral bioavailability of 24% may thus be an underestimate.

The CNS distribution of **CVN293** was determined in mice, rats, and monkeys. In rodents, brain to plasma ratios ranged from 0.72 to 1.85 and were generally consistent with time, indicating that equilibrium distribution is reached rapidly. Average $Kp_{u,u}$ values ranged from 0.6 to 1.4, demonstrating that **CVN293** freely distributes into the CNS in rodents. In line with this, CSF:unbound plasma values in rodents ranged from 0.7 to 1.1. In monkeys, CSF to plasma ratios ranged from 0.2 to 0.3 with corresponding $Kp_{u,u}$ values of 0.9 to 1.1, confirming that **CVN293** has a good CNS distribution in all species tested.

The KCNK13 inhibitory activity of **CVN293** is illustrated in Figure 3. In brief, **CVN293** fully reduced human KCNK13 mediated constitutive thallium influx, with a half maximal inhibitory concentration, $IC_{50}$ ± SD, of 41.0 ± 8.1 nM and maximal percent inhibition of 100.3 ± 1.4%. Similarly, equipotent inhibition was observed at mouse KCNK13, $IC_{50}$ = 28 ± 0.7 nM and maximal percent inhibition = 97 ± 1.8%. The selectivity of **CVN293** for KCNK13 was assessed by determining activity at two of the most closely related channels within the two-pore forming domain $K^+$ channel family—KCNK2 and KCNK6—which demonstrate 30−35% amino acid identity with KCNK13. In HEK-293 cells recombinantly expressing either human KCNK2 or KCNK6, **CVN293** (up to 30 $\mu$M) demonstrated minimal inhibition of constitutive thallium influx, with maximum inhibition at 30 $\mu$M of 17.4%


https://doi.org/10.1021/acsmedchemlett.4c00035
ACS Med. Chem. Lett. XXXX, XXX, XXX−XXX

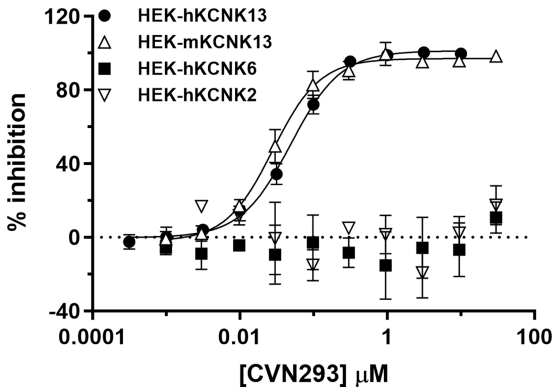


**Figure 3.** Inhibitory activity of **CVN293** for the human and mouse forms of KCNK13, KCNK2, and KCNK6. **CVN293** inhibitory activity was determined in HEK-293 cells expressing KCNK13, KCNK2, or KCNK6 in thallium flux assays. Data shown represent the averaged responses (initial slope; ± SD) normalized to controls from two independent experiments, each performed in duplicate.

(10.9%) and 10.7% (±8.9%) for KCNK2 and KCNK6, respectively.

In LPS-primed microglia isolated from neonatal mice, a low extracellular $K^+$ concentration stimulated $K^+$ efflux from the cells and promoted an NLRP3-dependent release of IL-1$\beta$ that is driven by KCNK13 currents.[7] In this cellular model, **CVN293** blocked the release of IL-1$\beta$ from microglia in a concentration-dependent manner, with a potency of 24 nM. **CVN293** reached a maximal inhibition of 59.1 ± 6.9% of the release of IL-1$\beta$ compared to that of vehicle (Figure 4A). Similarly, in mouse cultured hippocampal slices, **CVN293** (1 $\mu$M) attenuated the LPS/ATP-induced release of IL-1$\beta$ ($p < 0.001$) but was without effect in the LPS-alone stimulated system (Figure 4B and C). As $K^+$ efflux affects only the activation step of the NLRP3 inflammasome, these data confirm that KCNK13 has no role in the LPS-alone induced priming step of inflammasome activation.

Importantly, at 10 $\mu$M concentrations of **CVN293**, no activity was observed above 50% in a broad Eurofins promiscuity panel spanning 168 targets representing different protein classes. Further, this lead molecule showed a clean profile in a panel of cardiovascular targets (hERG, $Na_v1.5$, and $Ca_v1.2$) at the same concentration and was reported negative in preliminary assays addressing genotoxicity (data not shown).

The compounds described herein were prepared according to one of the two synthetic routes outlined in Scheme 1 for compounds **9**, **12**, and **13**. The experimental protocols for all final compounds are detailed in the Supporting Information. Importantly, all compounds with reported biological data were characterized by $^1H$ and $^{13}C$ NMR spectroscopy and high-resolution mass spectroscopy and displayed purity levels greater than 95% as determined by analytical HPLC. The first route was initiated with condensation of the diamine **21** and oxadiazole-3-carbimidoyl chloride **22** to give the fluoro-benzimidazole **23**. Subsequent substitution of the ring NH of the benzimidazole core led to a mixture of regioisomers **9** and **12**, which were separated by supercritical fluid chromatography. In the second route, a regioselective substitution of the more reactive fluorine atom adjacent to the nitro group of **24** provided the pyrazine intermediate **26**, and a *Béchamp* reduction followed by benzimidazole formation, as above, gave compound **13**.[10]

In summary, we herein describe the optimization of our previously reported KCNK13 inhibitors[7] culminating in the

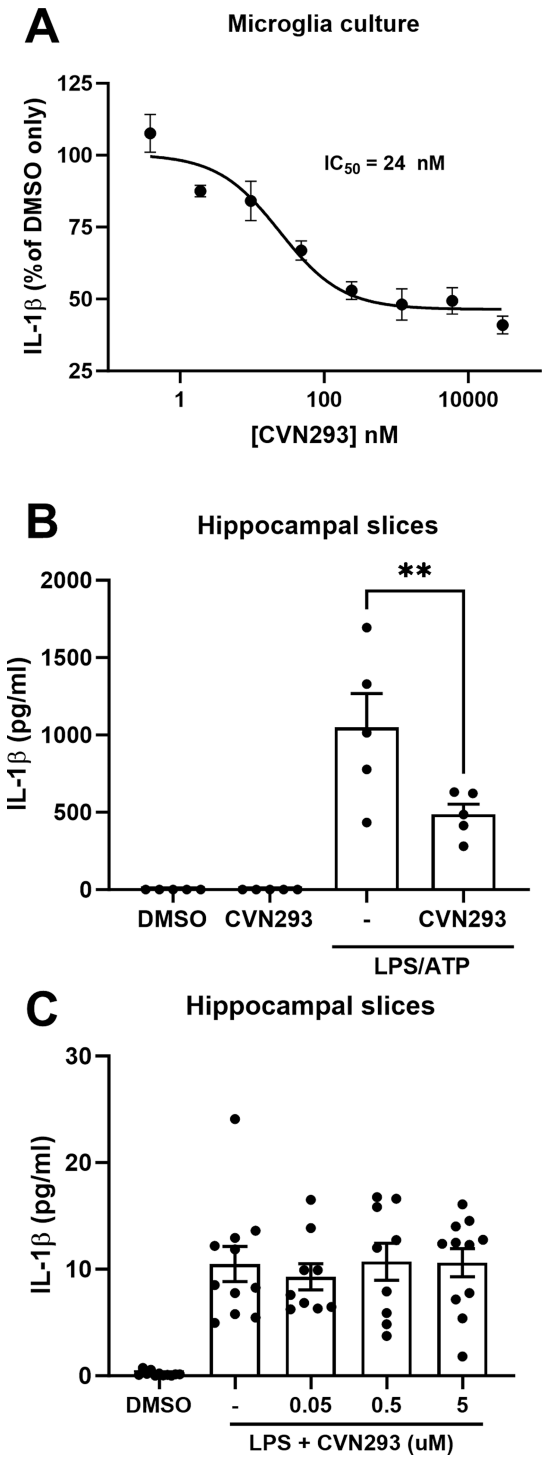


**Figure 4. CVN293** prevents IL-1$\beta$ release from murine microglia. Neonatal microglia cultures were primed with LPS and activated by the removal of extracellular $K^+$ (A) following the treatment with **CVN293**. Data are presented as a percentage of DMSO-treated cells and represent the mean ± SEM of five independent experiments. Data represent the mean ± SEM of five independent experiments. Statistical difference was calculated by two-way ANOVA followed by a multiple comparison with Tukey's model. Hippocampal slice cultures were primed with LPS with or without activation with ATP (5 mM) following the treatment with **CVN293** (1 $\mu$M; B and C). Data represent the mean ± SEM of at least five independent experiments. Statistical difference was calculated by one-way ANOVA followed by Dunnett's posthoc analysis. $^{**}P < 0.01$.


https://doi.org/10.1021/acsmedchemlett.4c00035
ACS Med. Chem. Lett. XXXX, XXX, XXX−XXX

**Scheme 1.** (a) EtOH, 80 °C, 40%; (b) $K_2CO_3$, DMF, RT, 25% **9**, 20% **12**; (c) $Et_3N$, $CH_3CN$, 90 °C, 70%; (d) $Fe^0$, $NH_4Cl$, EtOH, $H_2O$, 100 °C, 89%; (e) **22**, EtOH, 90 °C, 10%

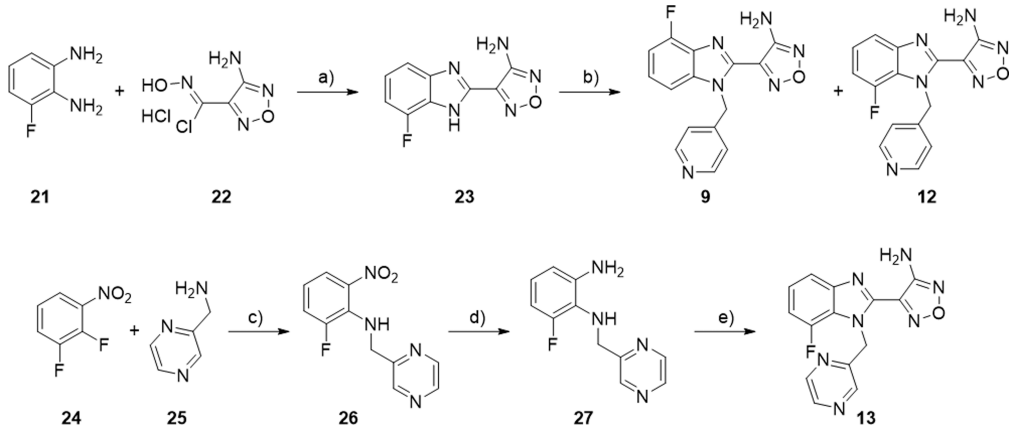


potent, selective, and brain permeable KCNK13 inhibitor **CVN293**, which is currently being investigated in phase 1 clinical trials. A key aspect of the optimization process was the improvement of metabolic stability and the pharmacokinetic profile of analogs, while retaining their KCNK13 inhibitory activity. Various replacements of the amino-oxadiazole moiety in compound **1** led to a significant loss in desired biological activity, but surprisingly, exchanging the polar exocyclic amino function for a methyl group retained potency. However, no benefit in metabolic stability was observed for methyl oxadiazole **4**. Only fluorine substituents were tolerated at the benzimidazole core without a loss of potency, whereas introduction of a second ring nitrogen in the pendant heterocycle group retained activity and, in some cases, led to markedly improved physicochemical properties and metabolic stability. For instance, the pyrazine **CVN293** combined excellent KCNK13 potency with good microsomal stability across species, solubility, and improved distribution to the CNS. The difluoro-analog **19** exhibited an even higher unbound brain concentration 4 h after a 10 mg/kg oral dosage. Unfortunately, this compound was less soluble than **CVN293** and showed significantly lower oral bioavailability in rat pharmacokinetic studies (see Supporting Information). We progressed **CVN293** to an in-depth preclinical evaluation. **CVN293** potently inhibits the NLRP3-inflammasome mediated production of the proinflammatory cytokine IL-1$\beta$ in microglia. In vivo efficacy in preclinical disease models and GLP safety data will be reported in due course. The molecule has been demonstrated to be selective across a broad panel of related and nonrelated targets, including those involved in cardiovascular function. The safety profile and biological characterization were commensurate with **CVN293** progressing into a phase 1 clinical assessment with the aim of evaluating its efficacy in neurodegenerative disease populations.

## EXPERIMENTAL PROCEDURES

All of the experimental procedures have been described in the Supporting Information.

## ASSOCIATED CONTENT

### Supporting Information

The Supporting Information is available free of charge at https://pubs.acs.org/doi/10.1021/acsmedchemlett.4c00035.

Methods for compound synthesis and analysis and for in vitro and in vivo procedures (PDF)

## AUTHOR INFORMATION


### Corresponding Author

**Lee A. Dawson** − *Cerevance Limited, Cambridge CB4 0PZ, United Kingdom*; Email: lee.dawson@cerevance.com

### Authors

**Roland W. Bürli** − *Cerevance Limited, Cambridge CB4 0PZ, United Kingdom*

**Kevin J. Doyle** − *Cerevance Limited, Cambridge CB4 0PZ, United Kingdom*

**Louise Dickson** − *Cerevance Limited, Cambridge CB4 0PZ, United Kingdom*; orcid.org/0000-0003-0550-7495

**Anna Rowland** − *Cerevance Limited, Cambridge CB4 0PZ, United Kingdom*

**Kim Matthews** − *Cerevance Limited, Cambridge CB4 0PZ, United Kingdom*

**Andrew J. Stott** − *Cerevance Limited, Cambridge CB4 0PZ, United Kingdom*

**Martin Teall** − *Cerevance Limited, Cambridge CB4 0PZ, United Kingdom*

**Bernardino Ossola** − *Cerevance Limited, Cambridge CB4 0PZ, United Kingdom*; orcid.org/0000-0002-5322-2614

**Samuel G. Russell** − *Cerevance Limited, Cambridge CB4 0PZ, United Kingdom*

**Jenna R. M. Harvey** − *Cerevance Limited, Cambridge CB4 0PZ, United Kingdom*

**Yiming Wu** − *Wuxi Apptec Co., Ltd., Waigaoqiao, Shanghai 200131, People's Republic of China*

**Lakshminarayana Narayana** − *Aragen Life Sciences Ltd, Bengaluru 562106, India*

**Nicola L. Brice** − *Cerevance Limited, Cambridge CB4 0PZ, United Kingdom*

**Mark Carlton** − *Cerevance Limited, Cambridge CB4 0PZ, United Kingdom*

Complete contact information is available at: https://pubs.acs.org/10.1021/acsmedchemlett.4c00035

### Author Contributions

[‖]These authors contributed equally. The manuscript was written through contributions of all authors. All authors have given approval to the final version of the manuscript. All authors except for Y.M. and L.N. were employees of Cerevance at the time of their contribution to this work.




https://doi.org/10.1021/acsmedchemlett.4c00035
ACS Med. Chem. Lett. XXXX, XXX, XXX−XXX

## Funding

These studies were funded by Cerevance Limited.

## Notes

The authors declare no competing financial interest.

## ■ ABBREVIATIONS

AD = Alzheimer's disease
ALS = amyotrophic lateral sclerosis
ANOVA = analysis of variance
BTB = brain tissue binding
BRCP = breast cancer resistance protein
CNS = central nervous system
CSF = cerebrospinal fluid
DAMPs = damage-associated molecular patterns
DMF = dimethylformamide
DMPK = drug metabolism and pharmacokinetics
DMSO = dimethyl sulfoxide
DNA = deoxyribonucleic acid
hERG = human ether-à-go-go-related gene
HLM = human liver microsomes
HPLC = high performance liquid chromatography
IL-1$\beta$ = interleukin 1 beta
KCNK13 = potassium two pore domain channel subfamily K member 13 gene
K2P = K+ two pore domain channel
$Kp_{brain}$ = brain plasma partition coefficient
$Kp_{uu}$ = unbound brain/plasma partition coefficient
LPS = lipopolysaccharide
MLM = mouse liver microsomes
MN = motor neurons
MND = motor neuron disease
MPO = multiparameter optimization
NETSseq = nuclear enriched transcript sort SEQuencing
NLRP3 = NLR family pyrin domain containing 3
NMR = nuclear magnetic resonance
PD = Parkinson's disease
PPB = plasma binding
PK = pharmacokinetic
RLM = rat liver microsomes
RNA = ribonucleic acid
RT = room temperature
SAR = structure activity relationship
SD = standard deviation
SEM = standard error of the mean
TDI = time dependent inhibition
THIK-1 = tandem pore domain halothane-inhibited K+ channel 1
TLR = toll-like receptor
UPLC = ultraperformance liquid chromatography
Vd = volume of distribution

## ■ REFERENCES

(1) Heneka, M. T.; McManus, R. M.; Latz, E. Inflammasome Signalling in Brain Function and Neurodegenerative Disease. *Nat. Rev. Neurosci.* **2018**, *19*, 610−621.
(2) Guan, Y.; Han, F. Key Mechanisms and Potential Targets of the NLRP3 Inflammasome in Neurodegenerative Diseases. *Front. Integr. Neurosci.* **2020**, *14*, 37.
(3) Schwaid, A. G.; Spencer, K. B. Strategies for Targeting the NLRP3 Inflammasome in the Clinical and Preclinical Space. *J. Med. Chem.* **2021**, *64* (1), 101−122.
(4) Madry, C.; Kyrargyri, V.; Arancibia-Ćarcamo, I. L.; Jolivet, R.; Kohsaka, S.; Bryan, R. M.; Attwell, D. Microglial ramification, surveillance, and interleukin-1$\beta$ release are regulated by the two-pore domain K+ channel THIK-1. *Neuron* **2018**, *97*, 299−312.
(5) Drinkall, S.; Lawrence, C. B.; Ossola, B.; Russell, S.; Bender, C.; Brice, N. B.; Dawson, L. A.; Harte, M.; Brough, D. The Two Pore Potassium Channel THIK-1 Regulates NLRP3 Inflammasome Activation. *Glia* **2022**, *70* (7), 1301−1316.
(6) Xu, X.; Stoyanova, E. I.; Lemiesz, A. E.; Xing, J.; Mash, D. C.; Heintz, N. Species and Cell-Type Properties of Classically Defined Human and Rodent Neurons and Glia. *Elife* **2018**, *7*, No. e37551.
(7) Ossola, B.; Rifat, A.; Rowland, A.; Hunter, H.; Drinkall, S.; Bender, C.; Hamlischer, M.; Teall, M.; Burley, R.; Barker, D. F.; Cadwalladr, D.; Dickson, L.; Lawrence, J. M. K.; Harvey, J. R. M.; Lizio, M.; Xu, X.; Kavanagh, E.; Cheung, T.; Sheardown, S.; Lawrence, C. B.; Harte, M.; Brough, D.; Madry, C.; Matthews, K.; Doyle, K.; Page, K.; Powell, J.; Brice, N. L.; Bürli, R. W.; Carlton, M. B.; Dawson, L. A. Characterisation of C101248: A Novel Selective THIK-1 Channel Inhibitor for the Modulation of Microglial NLRP3-Inflammasome. *Neuropharmacology* **2023**, *224*, 109330.
(8) Tang, H.; Sun, Y.; Fachim, H. A.; Cheung, T. K. D.; Reynolds, G. P.; Harte, M. K. Elevated Expression of Two Pore Potassium Channel THIK-1 in Alzheimer's Disease: An Inflammatory Mechanism. *Journal of Alzheimer's Disease* **2023**, *95* (4), 1757−1769.
(9) Couty, S.; Westwood, I. M.; Kalusa, A.; Cano, C.; Travers, J.; Boxall, K.; Chow, C. L.; Burns, S.; Schmitt, J.; Pickard, L.; Barillari, C.; McAndrew, P. C.; Clarke, P. A.; Linardopoulos, S.; Griffin, R. J.; Aherne, G. W.; Raynaud, F. I.; Workman, P.; Jones, K.; Van Montfort, R. L. M. The Discovery of Potent Ribosomal S6 Kinase Inhibitors by High throughput Screening and Structure-Guided Drug Design. *Oncotarget* **2013**, *4* (10), 1647−1661.
(10) Béchamp, A. J. De l'action des protosels de fer sur la nitronaphtaline et la nitrobenzine nouvelle méthode de formation des bases organiques artificielles de Zinin. *Ann. Chim. Phys.* **1854**, *42*, 186.


https://doi.org/10.1021/acsmedchemlett.4c00035
ACS Med. Chem. Lett. XXXX, XXX, XXX−XXX